JOURNAL OF GEOPHYSICAL RESEARCH: SPACE PHYSICS, VOL. 118, 3985–3994, doi:10.1002/jgra.50429, 2013

Propagation delay of solar wind discontinuities: Comparing different methods and evaluating the effect of wavelet denoising

C. Munteanu,[1,2,3] S. Haaland,[4,5] B. Mailyan,[6] M. Echim,[1,7] and K. Mursula[2]

Received 14 November 2012; revised 29 May 2013; accepted 30 June 2013; published 23 July 2013.

[1] We present a statistical study of the performance of three methods used to predict the propagation delay of solar wind structures. These methods are based on boundary normal estimations between the Advanced Composition Explorer (ACE) spacecraft orbiting the L1 libration point and the Cluster spacecraft near the Earth's magnetopause. The boundary normal estimation methods tested are the cross product method (CP), the minimum variance analysis of the magnetic field (MVAB), and the constrained minimum variance analysis (MVAB0). The estimated delay times are compared with the observed ones to obtain a quantitative measure of each method's accuracy. Boundary normal estimations of magnetic field structures embedded in the solar wind are known to be sensitive to small-scale fluctuations. Our study uses wavelet denoising to reduce the effect of these fluctuations. The influence of wavelet denoising on the performance of the three methods is also analyzed. We find that the free parameters of the three methods have to be adapted to each event in order to obtain accurate propagation delays. We also find that by using denoising parameters optimized to each event, 88% of our database of 356 events are estimated to arrive within ±2 min from the observed time delay with MVAB, 74% with CP, and 69% with the MVAB0 method. Our results show that wavelet denoising significantly improves the predictions of the propagation time delay of solar wind discontinuities.

Citation: Munteanu, C., S. Haaland, B. Mailyan, M. Echim, and K. Mursula (2013), Propagation delay of solar wind discontinuities: Comparing different methods and evaluating the effect of wavelet denoising, *J. Geophys. Res. Space Physics*, *118*, 3985–3994, doi:10.1002/jgra.50429.

1. Introduction

[2] Due to the lack of continuous monitoring of solar wind properties close to the Earth, solar wind measurements often need to be translated from an upstream monitor to the Earth's bow shock location. To accurately predict the propagation time of magnetic field structures embedded in the solar wind, one needs to take into account the orientation of the boundary normal of those structures. The challenge here is that most methods used to estimate these boundary normals are affected by small-scale fluctuations superposed on the magnetic field structure. Instead of using frequency filtering, which smears out the discontinuities and reduces the number of data points, we use wavelet denoising to reduce the effect of these fluctuations. Wavelet denoising is especially suited to remove low-amplitude high-frequency fluctuations while leaving the high-amplitude low-frequency parts of the signal unchanged.

[3] *Horbury et al.* [2001] used data from Advanced Composition Explorer (ACE) and Wind spacecrafts to study the propagation time of discontinuities characterized by southward interplanetary magnetic field (IMF) turnings. They showed that the best estimates of the propagation time were obtained when the orientation of discontinuities was calculated with the cross product method (CP), which assumes that the boundary normal is given by the cross product between the mean magnetic field upstream of the discontinuity and the mean magnetic field downstream of it.

[4] *Mailyan et al.* [2008] studied statistically the propagation time of about 200 IMF structures between ACE and Cluster. They computed the propagation time using four different methods: the flat delay method (FD), which assumes a constant convective motion of the structure along the Sun-Earth line, the CP method, the minimum variance analysis (MVAB), and the constrained minimum variance analysis (MVAB0) finding that the best results are obtained with MVAB0.

[5] *Pulkkinen and Rastätter* [2009] proposed a new method for computing the boundary normals of solar wind discontinuities. One of their motivations was the removal of the influence of small-scale fluctuations on the computed normals. Their method, based on MVAB0, uses a weight function to get smooth variations of the boundary normal,

[1]Institute of Space Sciences, Magurele, Romania.
[2]Department of Physics, University of Oulu, Oulu, Finland.
[3]Department of Physics, University of Bucharest, Magurele, Romania.
[4]Birkeland Center for Space Science, University of Bergen, Bergen, Norway.
[5]Max Planck Institute for Solar Systems Research, Lindau, Germany.
[6]Yerevan Physics Institute, Yerevan, Armenia.
[7]Belgian Institute for Space Aeronomy, Brussels, Belgium.

Corresponding author: C. Munteanu, Institute of Space Sciences, Atomistilor 409, P.O. Box MG-23, Bucharest-Magurele RO-077125, Romania. (costelm@spacescience.ro)

2169-9380/13/10.1002/jgra.50429

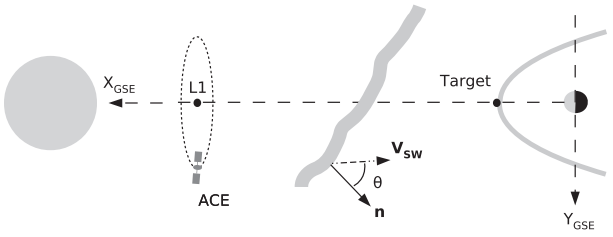

Figure 1. Illustration of a solar wind discontinuity propagating from ACE to Cluster (Target). Positions of the Sun, Earth, ACE and Cluster spacecraft, and the model discontinuity and its normal **n** at angle θ with respect to the solar wind velocity $\mathbf{V}_{SW}$ are shown. Note that this is just a sketch and both position and dimensions are not to scale (adapted from *Mailyan et al.* [2008]).

thus effectively low-pass filtering the computed normals. To test their time shift method, they used a global MHD model that computed the ground magnetic field. Although their method did provide some improvement in the timing of the modeled magnetic field, the improvements were not systematic and could not be detected in a statistical sample.

[6] *Haaland et al.* [2010] proposed a different approach of improving the boundary normal determination. They emphasized that the filtering should be performed on the input data rather than on the obtained normals. Also, instead of frequency filtering, they suggested the use of wavelet denoising, which was already tested on magnetic field measurements by *Haaland and Paschmann* [2001].

[7] Our study extends the analysis in *Mailyan et al.* [2008] by including the effect of wavelet denoising on the timing accuracy of three propagation delay estimation methods: CP, MVAB, and MVAB0. We also analyze the effect of varying the free parameters of the three methods on the timing accuracy.

[8] The paper is organized as follows. Section 2 presents the data sources and database of events. Section 3 discusses the time delay estimation methods. In section 4 we describe the approach adopted for wavelet denoising. Section 5 illustrates the results obtained for a case study, and section 6 gives the statistical results of the study. Section 7 summarizes the paper.

2. Data Description

[9] We use data from the ACE spacecraft in the solar wind and the Cluster spacecraft near the Earth's magnetopause. ACE orbits the L1 libration point at approximately 1.5×10^6 km upstream of the Earth. Cluster contains four identical satellites flying in close formation around the Earth. It has a 90° inclination elliptical polar orbit, with perigee at 4 R_E, apogee around 20 R_E, and orbital period of approximately 57 h. Cluster's apogee is in the upstream solar wind mainly from January to April every year, so our study will focus only on this period.

[10] In this work we use ACE magnetic field data from the MAG instrument [*Smith et al.*, 1998] at 16 s resolution and solar wind velocity data from the Solar Wind Electron, Proton, and Alpha Monitor instrument [*McComas et al.*,

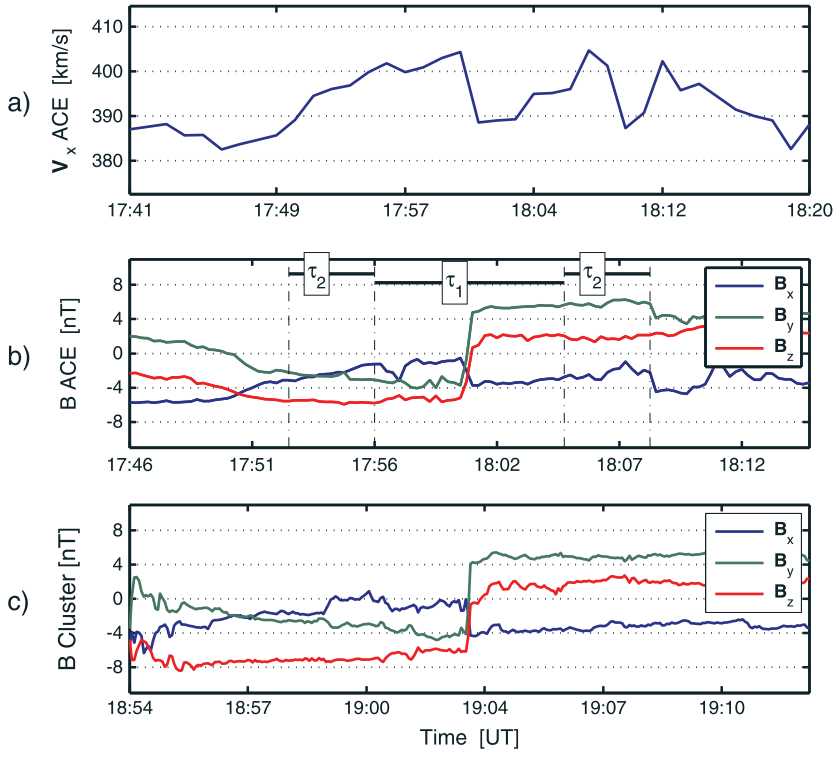

Figure 2. Sample IMF discontinuity observed by ACE and Cluster 3 on 06 January 2003: (a) *X* component of the solar wind velocity measured by ACE; (b) magnetic field components measured by ACE; (c) magnetic field components at C3 location. Figure 2b also depicts the time interval τ_1 = 8 min centered on the discontinuity and the time intervals τ_2 = 4 min on each side of τ_1, used in the cross product (CP) method. In Figures 2b and 2c, blue, green, and red lines indicate B_x, B_y, and B_z components of the IMF.

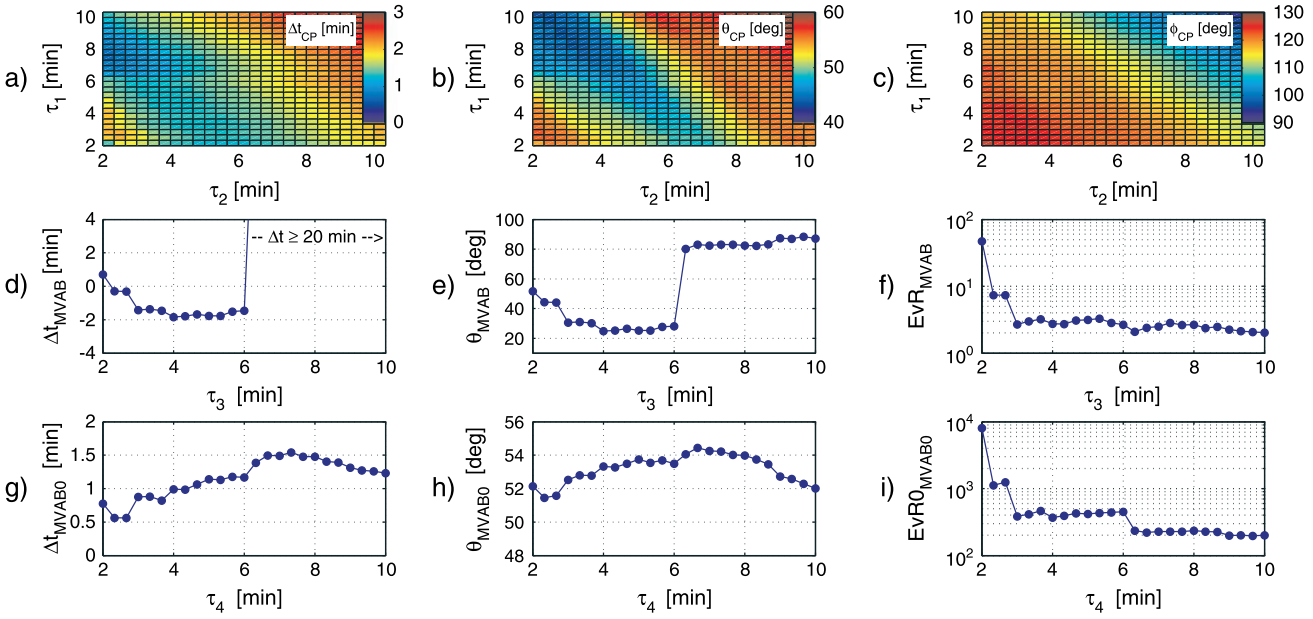

Figure 3. Illustration of the effect of varying the parameters of time delay estimation methods on the estimation accuracy and on the quality criteria of boundary normal estimation applied on the data from the 06 January 2003 event. The first row shows the CP method results: (a) the time delay estimation accuracy $\Delta t_{CP} = t_{CP} - t_{observed}$ as a function of τ_1 and τ_2, (b) the orientation angle θ_{CP} as a function of τ_1 and τ_2, and (c) the shear angle ϕ_{CP} (the angle between the mean upstream and downstream magnetic field vectors) as a function of τ_1 and τ_2. The second row shows the MVAB method results: (d) the time delay estimation accuracy Δt_{MVAB} as a function of τ_3, (e) the orientation angle θ_{MVAB} as a function of τ_3, and (f) the eigenvalue ratio EvR_{MVAB} as a function of τ_3. The third row shows the MVAB0 results: (g) the time delay estimation accuracy Δt_{MVAB0} as a function of τ_4, (h) the orientation angle θ_{MVAB0} as a function of τ_4, and (i) the eigenvalue ratio $EvR0_{MVAB0}$ as a function of τ_4.

1998] at 64 s resolution. Cluster data are from the Fluxgate Magnetometer (FGM—see *Balogh et al.*, 2001) and from the Cluster Ion Spectroscopy (CIS) experiment [*Rème et al.*, 2001], both at 4 s time resolution. Since we focus on the propagation delay of solar wind discontinuities between two points, most of the Cluster measurements are taken only from one spacecraft, Cluster 3, from now on referred as C3.

[11] Our database consists of 356 solar wind discontinuities observed by both ACE and C3 in the period 2001–2012. This database expands the data set used in *Mailyan et al.* [2008]. We first identified clear magnetic field rotations in C3 measurements by visually examining the Cluster summary plots. Since we focus on periods when C3 is in the upstream solar wind, we also examined the Cluster nominal position and the ion temperature (from the CIS experiment) to avoid any influences of bow shock processes (*Gosling et al.* [1978], *Paschmann et al.* [1981], and, for a recent review, *Burgess et al.* [2012]). Then we examined the ACE magnetic field measurements about an hour earlier in order to see if the same field rotation could be found there. Throughout the paper we will interchangeably use the terms "magnetic field structure," "magnetic field rotation," "directional discontinuity," or just "discontinuity." From a theoretical point of view this is not completely correct, but, for the purpose of our study, every amplitude change of at least 5 nT in less that $\sim$ 5 min in one or more components of the magnetic field is considered a discontinuity.

[12] All the satellite data were downloaded through the Automated Multi Dataset Analysis system (AMDA) [*Jacquey et al.*, 2010] (http://cdpp-amda.cesr.fr/DDHTML/index.html), a web-based facility for online data analysis of space physics data.

3. Time Delay Estimation Methods

[13] IMF discontinuities are considered to be locally planar structures tilted at arbitrary angles with respect to the Sun-Earth line. The configuration of a solar wind discontinuity propagating from ACE to C3 spacecraft is illustrated in Figure 1. The tilt of the discontinuity with respect to the flow direction, referred to as θ angle, and the displacement of the two satellites from the Sun-Earth line can have an important influence on the estimated time delay between the two satellites. Assuming that the radial propagation speed of the discontinuity is given by the projection of the solar wind velocity vector $\mathbf{V}_{SW}$ onto the boundary normal direction $\mathbf{n}$ and that the relative distance between the two observation points with respect to the discontinuity is the observed distance $\mathbf{D}$ projected onto $\mathbf{n}$, the time delay dt between the two points is given by

$$dt = \frac{\mathbf{D} \cdot \mathbf{n}}{\mathbf{V}_{SW} \cdot \mathbf{n}}. \quad (1)$$

We use here three boundary normal estimation methods : CP, MVAB, and MVAB0 (as in *Mailyan et al.* [2008]). The CP method assumes that the discontinuity normal is given by the cross product between the mean upstream magnetic field $\mathbf{B}_1$

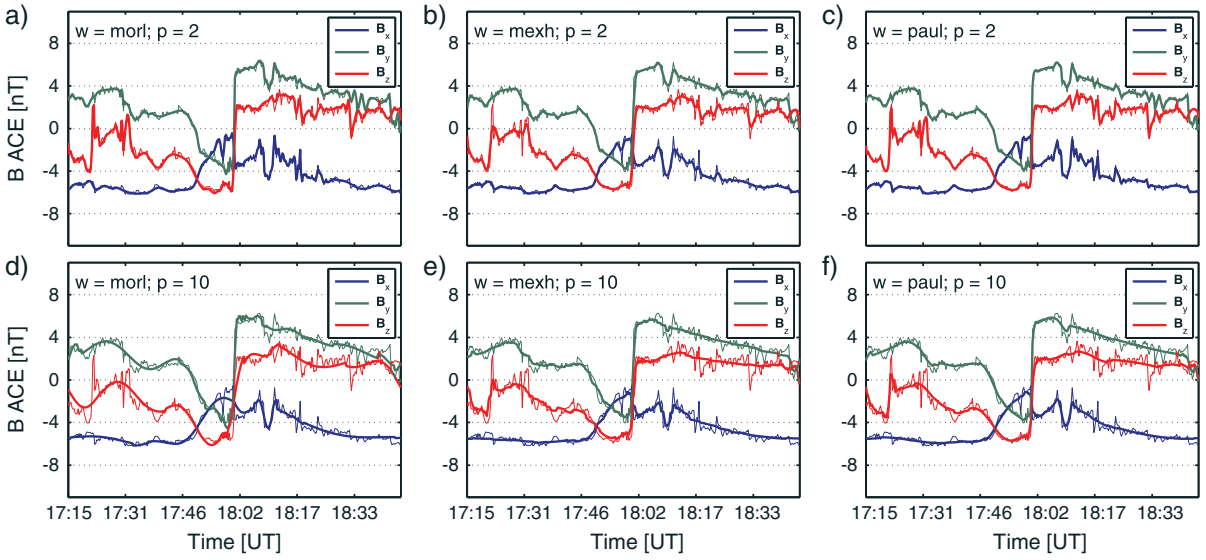

Figure 4. Illustration of wavelet denoising for the event on 06 January 2003. Shown are the denoising results for the Morlet wavelet function at the threshold levels (a) p = 2 and (d) p = 10, the Mexican Hat wavelet at (b) p = 2 and (e) p = 10, and Paul wavelet at (c) p = 2 and (f) p = 10. Blue, green, and red lines indicate original (thin lines) and denoised (thick lines) $\mathbf{B}_x$, $\mathbf{B}_y$, and $\mathbf{B}_z$ components of the magnetic field measured by ACE.

and the mean downstream magnetic field $\mathbf{B}_2$ [*Colburn and Sonett*, 1966]:

$$\mathbf{n}_{\mathrm{CP}} = \frac{\mathbf{B}_1 \times \mathbf{B}_2}{|\mathbf{B}_1 \times \mathbf{B}_2|}. \tag{2}$$

Strictly speaking, equation (2) is valid only in case of tangential or quasi-tangential discontinuities (TDs), i.e., planar structures with zero magnetic field along the normal [*Colburn and Sonett*, 1966]. The use of the CP method is justified by the fact that the large majority of our discontinuities have a small magnetic field normal component (as shown in Figure 11 along with other results). To compute the two vectors, we need to set two time intervals: τ_1 and τ_2. The time interval τ_1 is centered on the discontinuity with its left margin coinciding with the end point of a time interval of length τ_2 over which the average field at "left," $\mathbf{B}_1$, is computed. The right margin of τ_1 coincides with the first point of a time interval of length τ_2 over which the average field at "right,-" $\mathbf{B}_2$, is computed (see Figure 2 for a graphical representation of the two time intervals). The uncertainty in boundary normal estimation increases with increasing collinearity between $\mathbf{B}_1$ and $\mathbf{B}_2$ [*Knetter*, 2005]. The shear angle ϕ, i.e., the angle between $\mathbf{B}_1$ and $\mathbf{B}_2$, and the θ angle can be used as quality factors for the normal estimation. *Mailyan et al.* [2008] showed that values of θ larger than $\sim 70°$ can lead to erroneous time delay estimations.

[14] MVAB is the most frequently used method to obtain the orientation of a planar magnetic field structure [see, e.g., *Sonnerup and Scheible*, 1998]. One first computes the eigenvectors and eigenvalues of the covariance matrix of magnetic field measurements, $\mathbf{M}_{\nu\mu}$:

$$\mathbf{M}_{\nu\mu} = \langle B_\mu B_\nu \rangle - \langle B_\mu \rangle \langle B_\nu \rangle, \tag{3}$$

where $\langle ... \rangle$ denotes averaging over a certain time interval centered on the discontinuity, indicated here as τ_3. The eigenvector corresponding to the smallest eigenvalue is used as an estimator for the boundary normal $\mathbf{n}_{\mathrm{MVAB}}$. The ratio between the intermediate and minimum eigenvalues, called EvR_{MVAB}, and the θ angle can be used as quality factors of the normal estimation [*Mailyan et al.*, 2008].

[15] Previous studies about solar wind discontinuities suggest that most of them resemble TDs [*Knetter*, 2005]. Knowing this, we can estimate the boundary normal using the constrained minimum variance analysis (MVAB0), where the normal magnetic field is zero by definition [*Sonnerup and Scheible*, 1998]. In MVAB0, the covariance matrix $\mathbf{M}_{\nu\mu}$ (equation (3)) is replaced by

$$\mathbf{Q}' = \mathbf{P}_{ik} M_{\nu\mu} \mathbf{P}_{nj} \text{ with : } \mathbf{P}_{ij} = \delta_{ij} - \mathbf{b}_i \mathbf{b}_j, \tag{4}$$

where $\delta_{ij} = 1$ for $i = j$ and 0 otherwise, and $\mathbf{b} = \langle \mathbf{B} \rangle / |\langle \mathbf{B} \rangle|$ is the direction of the average magnetic field. The time interval τ_4 centered on the discontinuity and used to calculate the covariance matrix $\mathbf{Q}'$ is a free parameter in MVAB0. The eigenvalues and eigenvectors of $\mathbf{Q}'$ have now a different meaning: the lowest eigenvalue is zero, and its corresponding eigenvector is $\mathbf{b}$. The eigenvector corresponding to the lowest nonzero eigenvalue is now the normal estimator $\mathbf{n}_{\mathrm{MVAB0}}$. The ratio between the maximum and intermediate eigenvalues, called $EvR0_{\mathrm{MVAB0}}$, and the θ angle can be used as quality factors of the normal estimation [*Mailyan et al.*, 2008].

[16] The results from the above mentioned three methods are also compared with the results obtained assuming a simple convective motion of discontinuities along the Sun-Earth line, referred to in the literature as the flat delay method (FD) [*Mailyan et al.*, 2008]. Here, the time delay between the two observation points is given by

$$dt_{\mathrm{FD}} = \frac{\mathbf{D}_x}{\mathbf{V}_x}, \tag{5}$$

where $\mathbf{D}_x$ is the $\mathbf{X}_{\mathrm{GSE}}$ component of the distance $\mathbf{D}$ between ACE and C3 and $\mathbf{V}_x$ is the $\mathbf{X}_{\mathrm{GSE}}$ component of the solar wind velocity vector $\mathbf{V}_{\mathrm{SW}}$.

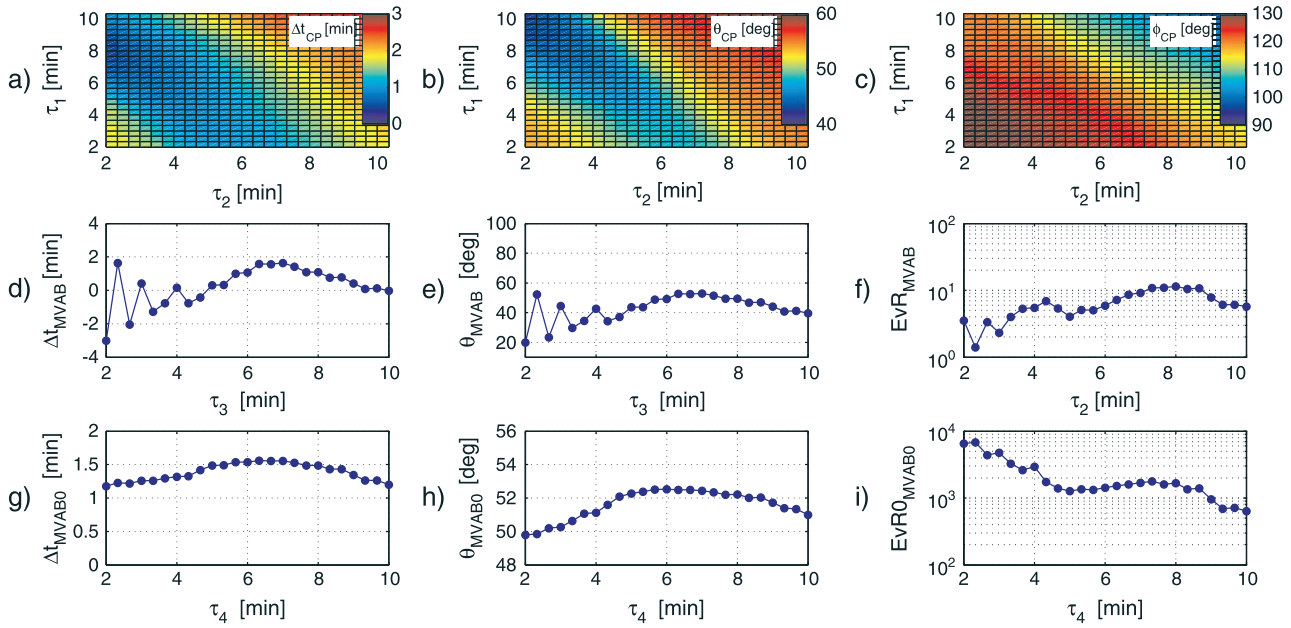

Figure 5. Illustration of the effect of model parameters on the accuracy of time delay estimation and quality criteria for the wavelet denoised data (Morlet, $p = 10$) shown in Figure 4d. The format is the same as in Figure 3.

4. Wavelet Denoising

[17] Wavelet denoising is a powerful technique bearing similarities with frequency filtering. Instead of removing frequency components from the signal, wavelet denoising removes certain wavelet coefficients based on their amplitude. The continuous wavelet transform of a time series $f(t)$ is

$$T(a,b) = \int_{-\infty}^{\infty} f(t)\psi^{a,b}(t)\,\mathrm{d}t, \quad \text{with} \quad \psi^{a,b}(t) = a^{-1/2}\psi\left(\frac{t-b}{a}\right), \quad (6)$$

where a is the scale parameter, b is the translation parameter, ψ is the wavelet mother function, and $T(a,b)$ is the wavelet coefficients matrix (see, e.g., *Daubechies* [1992] for more details).

[18] The large-amplitude low-frequency components of the time series and the low-amplitude high-frequency ones (the "noise") are occupying different amplitude ranges in the coefficients matrix $T(a,b)$. Our study uses hard thresholding as a wavelet denoising method, in which all wavelet coefficients below a certain amplitude level are set to zero. The threshold amplitude level p is defined here as a percentage of the total amplitude range of the coefficients matrix. For example, a denoising with $p = 0$ leaves the time series unchanged while a denoising with $p = 10$ sets to zero all coefficients with amplitudes smaller than 10% of the total amplitude range of the matrix $T(a,b)$. The resulting wavelet coefficients are defined as

$$T^d(a,b) = \begin{cases} T(a,b) & , \text{if } |T(a,b)| > (p/100)\cdot\max(|T(a,b)|), \\ 0 & , \text{if } |T(a,b)| \le (p/100)\cdot\max(|T(a,b)|). \end{cases} \quad (7)$$

There is also the possibility of using soft thresholding, where all wavelet coefficients are translated toward zero by the amount $(p/100)\cdot\max(|T(a,b)|)$ [*Donoho*, 1995]. The soft thresholding technique was devised in order to preserve the smoothness of the original signal after denoising. Since we are interested only in preserving the sharp discontinuities, the hard thresholding method is more appropriate.

[19] Because the continuous wavelet transform is redundant, there is no unique way of defining a reconstruction formula. The inverse continuous wavelet transform is presented classically in the double integral form:

$$f^d(t) = C_\psi \int_a \int_b a^{-2} T^d(a,b)\psi^{a,b}(t)\,\mathrm{d}a\,\mathrm{d}b, \quad (8)$$

where C_ψ is a constant depending only on the wavelet mother function ψ (empirically derived values of C_ψ for some commonly used wavelet functions are given in *Torrence and Compo* [1998]).

[20] An important factor to be considered in wavelet analysis is the wavelet shape, which should reflect the type of features present in the time series. We tested three families of wavelets: Morlet, known to be accurate in the frequency domain, Paul that has a good time resolution, and the second derivative of a Gaussian, also known as the Mexican Hat wavelet, that has lower frequency and time resolutions [*De Moortel et al.*, 2004]). Since our denoising thresholds are very low, i.e., only a small fraction of the signal is removed, properties such as frequency and time resolution will not have a profound effect on the reconstructed time signal. The effects of the wavelet basis on the denoising are discussed in sections 5 and 6.

[21] As used here, wavelet denoising has two free parameters: the wavelet function ψ and the threshold level p. Values of p larger than ~ 10 lead to the smearing out of discontinuities; therefore, the maximum value of p is set to 10. This is by no means the only way of denoising a time series using wavelet-based algorithms, and we plan to extend our study in subsequent papers by testing other denoising schemes. The denoising procedure described above is applied independently to each of the three components of the magnetic

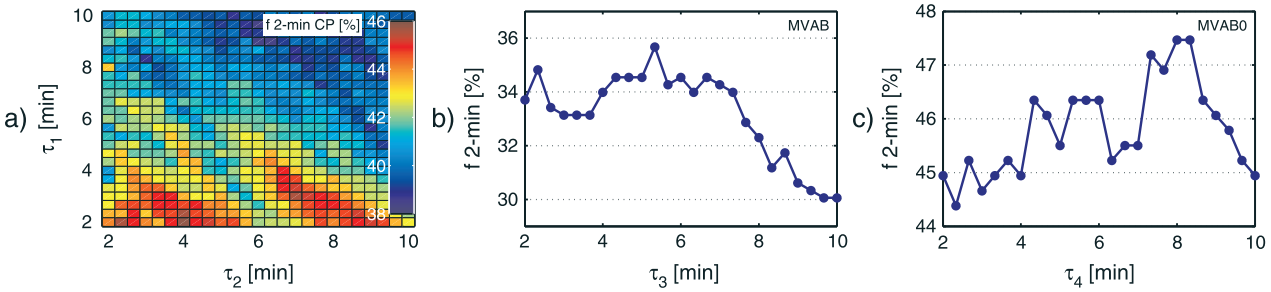

Figure 6. The fraction of discontinuities with time delay accuracy Δt within ± 2 min, $f_{2\text{–min}}$, as a function of method parameters: $f_{2\text{–min}}$ for (a) CP as a function τ_1 and τ_2, (b) for MVAB as a function τ_3, and (c) for MVAB0 as a function of τ_4. The parameters that maximize the 2 min fractions are ${\tau_1}^m = 2$ min and ${\tau_2}^m = 4$ min for CP, and ${\tau_3}^m = 5.33$ min and ${\tau_4}^m = 8.33$ min for MVAB and MVAB0, respectively.

field. Further details about wavelet denoising can be found in *Donoho and Johnstone* [1995], *Donoho* [1995], and *Donoho et al.* [1995].

5. Case Study, 6 January 2003

[22] Figure 2 shows a sample discontinuity observed by ACE at 18:01 UT on 06 January 2003. Figures 2a and 2b depict the X component of the solar wind velocity and the magnetic field measured by ACE respectively, while the magnetic field measurements of the same discontinuity detected by C3 at 19:03 UT are shown in Figure 2c. The observed time delay, dt_{obs}, between ACE and C3 is in this case 62 min.

[23] We have computed the time delay accuracy $\Delta t_{\text{met}} = dt_{\text{met}} - dt_{\text{obs}}$, where dt_{met} is the time delay estimated using one of the three methods (CP, MVAB, or MVAB0), and also the related quality factors (θ_{met}, ϕ_{CP}, EvR_{MVAB}, and $EvR0_{\text{MVAB0}}$). The results are shown in Figure 3. The parameters τ_1, τ_2, τ_3, and τ_4 are varied from 2 to 10 min, with a step size of 1/3 min $\approx$ 0.33 min. The choice of the 1/3 min (20 s) time step is motivated mainly by the time resolution of ACE magnetic field data (16 s). If we had used an increment of 1/4 min (15 s), the time step would have been smaller than the time resolution of the data, and this would have introduced unnecessary and redundant computations. A step size of 20 s assures that every increment corresponds to adding at least one data point to the computations. The best result for CP is obtained when $\tau_1 = 7.33$ min and $\tau_2 = 2$ min, corresponding to a minimum in $|\Delta t_{\text{CP}}|$ of ~ 35 s. We see that good accuracy (values of $|\Delta t_{\text{CP}}|$ smaller than 2 min) corresponds to fairly small values of θ_{CP} and relatively large values of the quality factor ϕ. Figure 3 shows that, in the case of this discontinuity, values of θ_{CP} larger than about 55° and ϕ smaller than 115° correspond to large values of $|\Delta t_{\text{CP}}|$, i.e., small accuracy of time delay estimation.

[24] Figure 3 also presents the results for Δt_{MVAB} (Δt_{MVAB0}), θ_{MVAB} (θ_{MVAB0}), and EvR ($EvR0$) as a function of τ_3 (τ_4). The best results are obtained for $\tau_3 = \tau_4 = 2.33$ min, which give a minimum $|\Delta t|$ of ~ 30 s. The sharp separation in MVAB between accurate time delay predictions for values of $\tau_3 \leq 6$ min and highly inaccurate ones for $\tau_3 > 6$ min

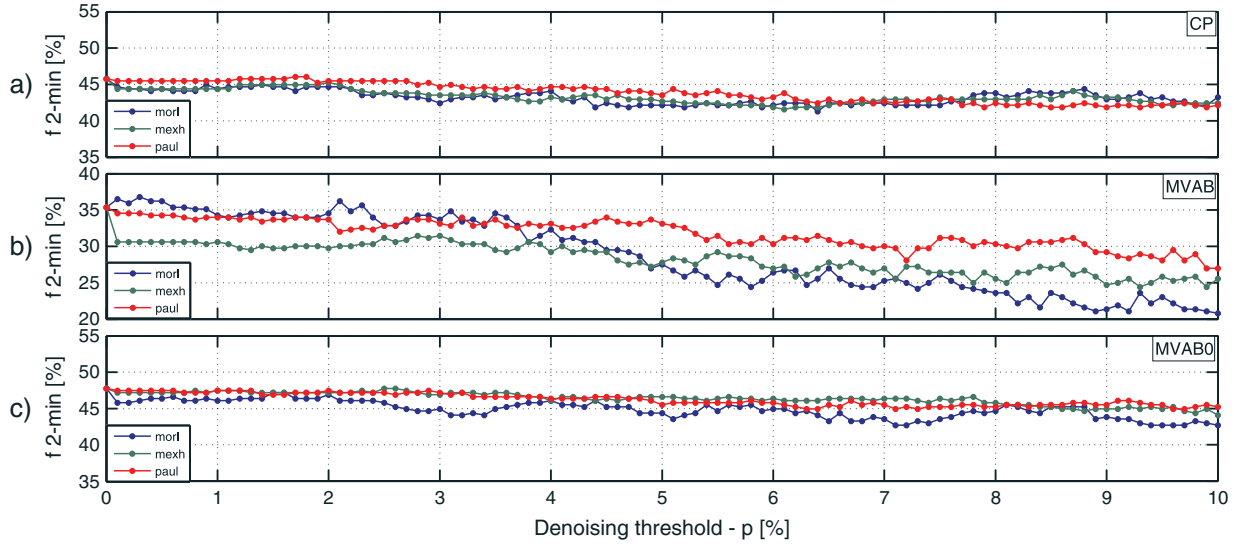

Figure 7. $f_{2\text{–min}}$ for the three time delay estimation methods as a function of threshold amplitude level for (a) CP, (b) MVAB, and (c) MVAB0. The method parameters used in the calculations are ${\tau_1}^m$, ${\tau_2}^m$, ${\tau_3}^m$, and ${\tau_4}^m$. The blue, green, and red lines indicate the wavelet functions Morlet, Mexican Hat, and Paul, respectively.

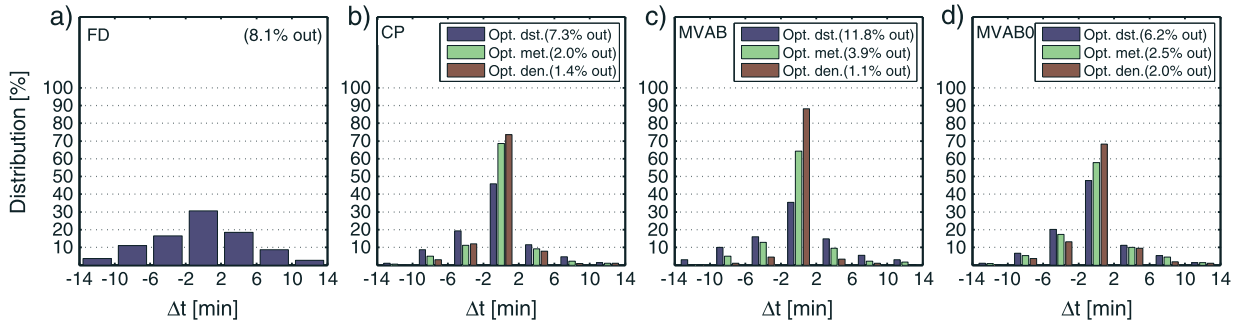

Figure 8. Distributions of time delay accuracy Δt for (b) CP, (c) MVAB, and (d) MVAB0 obtained using the method parameters that maximize the 2 min fractions presented in Figure 6 (Opt. dst., blue bins), the individually optimized method parameters (Opt. met., green bins), and the individually optimized denoising parameters (Opt. den., red bins). Also shown is the (a) histogram of time delay accuracy obtained with the FD method. The percentage of discontinuities outside the ± 14 min interval for Δt are shown in the top right corner for each method.

is due to the rapid decrease in the B_x component around 17:57 UT, which is included in estimates using $\tau_3 > 6$ min. MVAB0 is much less influenced by the presence of the sharp decrease in B_x, leading to a more smooth dependence of $\Delta t_{\mathrm{MVAB0}}$ and θ_{MVAB0} on τ_4. Using values larger than 6 min for the parameter τ_3, the quality factor θ_{MVAB} increases abruptly to values larger than 80°, and EvR_{MVAB} decreases to values smaller than 2. This shows that, in the case of this discontinuity, poor time delay accuracy corresponds to large values of θ_{MVAB} and small values for EvR_{MVAB}.

[25] Figure 4 shows the denoised magnetic field superimposed on the original time series for the three wavelet functions mentioned in the previous section and two threshold levels, p = 2 and p = 10. We see that the threshold level has a more important effect on the results than the wavelet function (see also Figure 7). We also see that denoising with p = 10, for all wavelet bases, removes the sharp decrease in B_x (at 17:57 UT) responsible for the erroneous time delays obtained using $\tau_3 > 6$ min.

[26] Figure 5 shows an analysis similar to the one presented in Figure 3 using the denoised time series presented in Figure 4d (Morlet wavelet function and threshold level p = 10). While denoising leaves the results of CP and MVAB0 largely unchanged, the MVAB results are significantly improved. The MVAB method applied on denoised data predicts now a correct time delay (with an accuracy within ± 2 min) for all values of the parameter τ_3 between 2 to 10 min. Denoising also increases the eigenvalue ratio EvR_{MVAB}, thus allowing the use of increased lower limits for this quality factor, resulting in a better overall data quality.

6. Statistical Results

[27] Figure 6 shows how the fraction of discontinuities with accurate time delay estimation (i.e., within ± 2 min, indicated as $f_{2\text{–min}}$) varies as a function of method parameters, for each of the three methods. The $f_{2\text{–min}}$ were computed with τ_1, τ_2, τ_3, and τ_4 ranging from 2 to 10 min with the

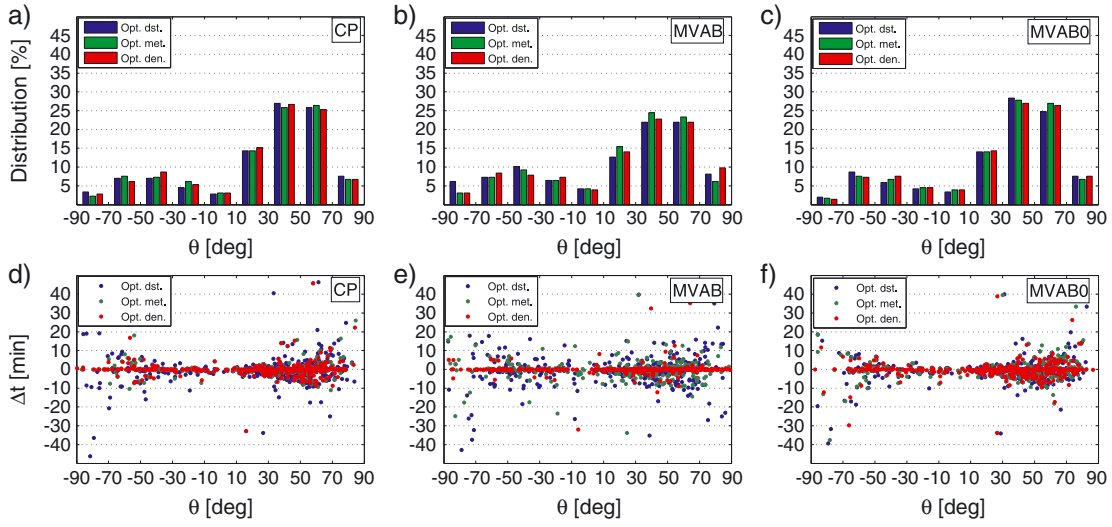

Figure 9. Illustration of the influence of wavelet denoising on the orientation angle θ. (top) Histograms of θ angles for (a) CP, (b) MVAB, and (c) MVAB0. (bottom) Time delay accuracy Δt as a function of θ for (d) CP, (e) MVAB, and (f) MVAB0. Blue, green, and red colors have the same meaning as in Figure 8.

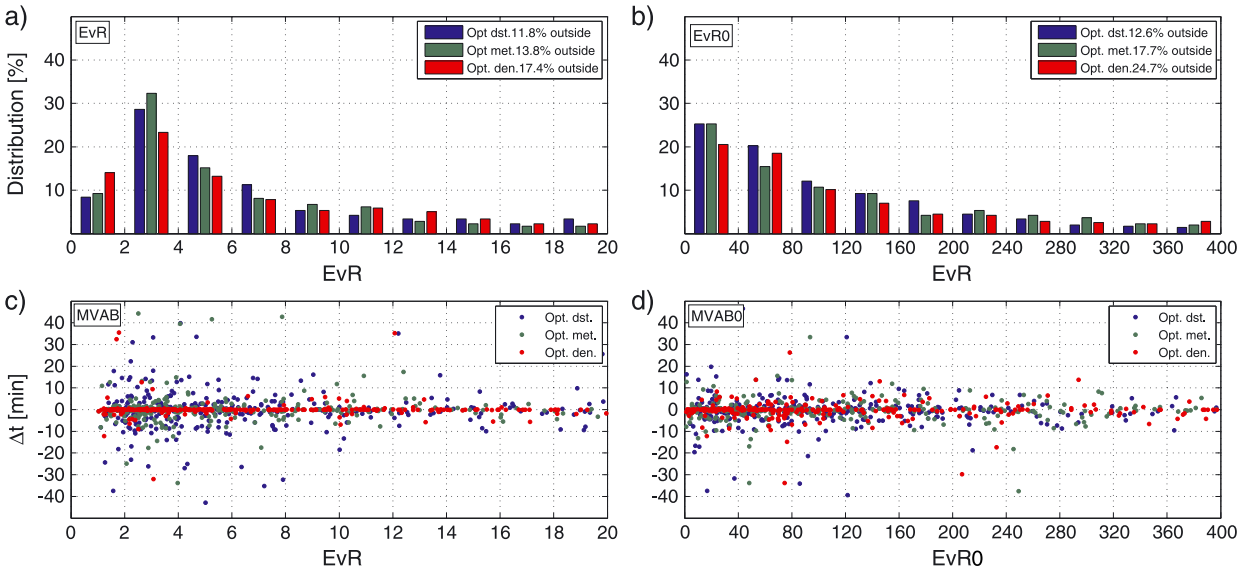

Figure 10. Illustration of the influence of wavelet denoising on the eigenvalue ratios EvR and EvR0, computed with MVAB and MVAB0, respectively. (top) Histograms of (left) EvR and (right) EvR0. (bottom) Time delay accuracy Δt as a function of (left) EvR and (right) EvR0. Blue, green, and red colors have the same meaning as in Figure 8.

same time step as described in the previous section (20 s). The parameters that maximize $f_{2\text{–min}}$ are $\tau_1{}^m$ = 2 min, $\tau_2{}^m$ = 4 min, $\tau_3{}^m$ = 5.33 min, and $\tau_4{}^m$ = 8.33 min. Using this set of parameters, 45% of discontinuities are estimated within ±2 min from the observed times for CP, 35.5% for MVAB and 47.5% for MVAB0. The accuracy of time delay estimation improves when a shorter τ_1 is used in CP, decreases when increasing τ_3 in MVAB, and is relatively constant when varying τ_4 for MVAB0. In each case we obtain only modest fractions of accurate time delay estimations (below 50%) regardless of the set of parameters used. A similar optimization procedure was used by *Weimer and King* [2008] to determine the optimum set of parameters for CP and MVAB0. They found that the best results are obtained if τ_1 = 0 min, τ_2 = 2.13 min, and τ_4 = 6.66 min and that the estimation accuracies are relatively equal for the two methods. *Mailyan et al.* [2008] used the set of parameters: τ_1 = 7 min, τ_2 = 2.66 min, and τ_3 = τ_4 = 7 min and determined that the best results are obtained with the MVAB0 method.

[28] Figure 7 depicts the $f_{2\text{–min}}$ computed with $\tau_1{}^m$, $\tau_2{}^m$, $\tau_3{}^m$, and $\tau_4{}^m$ and different wavelet functions as a function of denoising threshold level p. The wavelet functions tested are Morlet (blue), Mexican Hat (green), and Paul (red line); the threshold level p is varied from 0 to 10, with a step size of 0.1. For example, the first point of the green line in Figure 7a represents the $f_{2\text{–min}}$ computed using $\tau_1{}^m$ and $\tau_2{}^m$ in the CP method for all discontinuities, the second point is computed by first denoising the time series used as input in CP with the Mexican Hat wavelet and a threshold p = 0.1 and then calculating $f_{2\text{–min}}$ as above, the third point is computed with a threshold p = 0.2, and so on. Figure 7 shows that the three methods are quite stable to small values of p, but a clear decreasing trend is seen as p increases. For CP and MVAB0 the decreasing trend is reduced compared with the MVAB method, and also the variability of $f_{2\text{–min}}$ is slightly lower for CP and MVAB0. A notable result is obtained for MVAB using the Morlet wavelet, where we see that up to p ≈ 3, $f_{2\text{–min}}$ is clearly above the values corresponding to the other two wavelet functions; between p = 3 and p = 5 the values of $f_{2\text{–min}}$ are comparable, and above p = 5 the values obtained with MVAB are lower than the ones for the other two wavelet functions. This effect may be due to the lower temporal resolution of the Morlet wavelets that are able to filter out more efficiently the high-frequency fluctuations, leading thus to the smearing out of the sharp discontinuities. Figure 7 also shows that by using the same set of denoising parameters for all discontinuities, the fraction of accurate time delay estimations shows only a very small increase for small values of the threshold parameter p, if at all.

[29] In order to calculate the optimum parameters of the boundary normal estimation methods for each event individually, we varied τ_1, τ_2, τ_3, and τ_4 from 2 to 10 min, with a step size of 20 s, and determined those values that minimize the time delay accuracy $|\Delta t|$ (as in Figure 3). Figure 8 shows the distribution of Δt for each method in the case of optimized method parameters (Opt. met., indicated as green bins). It is clear that the percentages of accurate time delay estimations are significantly improved. As a matter of fact, $f_{2\text{–min}}$ increased up to 69% for CP, 65% for MVAB, and 59% for MVAB0.

[30] Then we determined the optimum set of denoising parameters for each discontinuity individually. The optimization procedure is similar to the one applied to optimize the method parameters. To optimize the set of denoising parameters, we use the optimum method parameters for each discontinuity and then compute the time delays for different denoising parameters. The optimum set of denoising parameters is the one that maximizes the prediction accuracy. The distributions of Δt in this case are presented in Figure 8 as red bins indicated as "Opt. den." and clearly show that the $f_{2\text{–min}}$ increases up to 74% for CP, 88% for MVAB, and

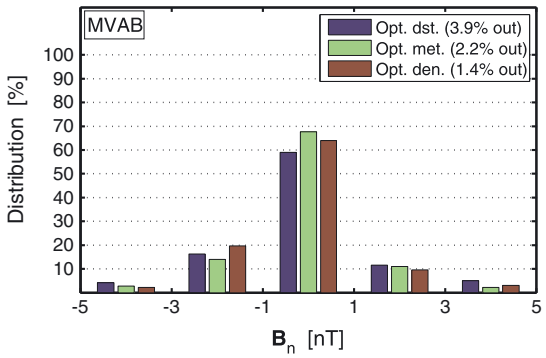

Figure 11. Illustration of the influence of wavelet denoising on the mean magnetic field along the boundary normal, $\mathbf{B}_n$, computed with MVAB. (top right corner) The percentage of discontinuities with $\mathbf{B}_n$ outside the ± 5 nT interval. Blue, green, and red colors have the same meaning as in Figure 8.

69% for MVAB0. The rather small improvement for CP was expected since a high accuracy was already obtained by individually optimizing the method parameters. In the case of MVAB0 the wavelet denoising increases the 2 min fraction, but a relatively large number of discontinuities still remain outside the ± 2 min interval. The main result in Figure 8 is the improvement in the case of individually optimized denoising parameters for MVAB, for which almost 99% of discontinuities are now estimated with an accuracy within ± 6 min. Figure 8 also shows the results obtained with the fixed set of parameters that maximize $f_{2\text{–min}}$ (indicated as Opt. dst.) inferred from the results of Figure 6 ($\tau_1{}^m$, $\tau_2{}^m$, $\tau_3{}^m$, and $\tau_4{}^m$). We see that $f_{2\text{–min}}$ for MVAB obtained using individually optimized denoising parameters is more than 50% larger that the corresponding fraction obtained with the fixed set of parameters above.

[31] Figure 8a illustrates the results obtained with the FD method. As expected, the prediction accuracy of FD is rather poor compared with the other three methods, and only 30% of events are predicted with a time delay accuracy Δt within ± 2 min.

[32] We also studied the influence of wavelet denoising on the statistics of discontinuity orientation for the three methods. The results are presented in Figure 9. We have already seen in Figures 3 and 5 that the orientation angles θ are influenced by denoising for individual cases, but we now see that the distribution is not significantly affected. The time delay estimation accuracy for MVAB is improved by denoising without significantly modifying the distribution of θ angles. This shows that time delay can be accurately estimated using the MVAB method if a proper preliminary denoising is performed, even if the plane of the discontinuity is almost parallel to the Sun-Earth line (θ angles close to $\pm 90°$). In the case of CP and MVAB0 methods, we see a large scatter in timing accuracy for values of θ larger than $\sim 50°$, even for the optimum denoising case. This means that discontinuities with large θ angles are predicted less accurately than the ones with small angles. A similar result was reported in *Mailyan et al.* [2008], which concluded that an acceptable maximum value for θ, for an accurate normal estimation, is 70°.

[33] We studied also the influence of wavelet denoising on the statistics of field rotation angles ϕ calculated with the CP method. The denoising procedure has no significant influence on the distribution of ϕ angles, so we decided not to show it.

[34] Figure 10 presents the influence of wavelet denoising on the eigenvalue ratios for MVAB and MVAB0. The EvR distribution is not significantly affected by denoising, and the time delay accuracy is improved irrespective of the EvR value, contrary to the other two cases (Opt. dst. and Opt. met.) where better results are obtained for eigenvalue ratios above ~ 8. The EvR0 distributions show that the number of discontinuities with EvR0 larger than 400 is doubled after denoising, compared with the results obtained for Opt. dst. We see that the time delay accuracy is improved after denoising irrespective of EvR0.

[35] We also studied the influence of wavelet denoising on the mean magnetic field along the boundary normal computed with MVAB. The results are presented in Figure 11. Using the parameter $\tau_3{}^m$, we find that 59% of discontinuities are estimated to have a $\mathbf{B}_n$ component in the ± 1 nT interval and 3.9% are outside the ± 5 nT interval. Using the individually optimized method parameters (Opt. met.), we find that 68% are now in the ± 1 nT interval and only 2.2% are outside the ± 5 nT interval. For the individually optimized denoising parameters (Opt. den.), 64% are in the ± 1 nT interval and only 1.4% are outside the ± 5 nT interval. These results show that even before denoising the majority of discontinuities in our database had a very small normal component of the magnetic field and denoising only slightly increases this number. The small normal component of the magnetic field indicates that most of the discontinuities in our database resemble tangential discontinuities.

7. Summary and Conclusions

[36] We have presented a statistical analysis of the performance of three methods (CP, MVAB, and MVAB0) to compute the propagation delay of solar wind discontinuities and the influence of wavelet denoising on this performance. We analyzed 356 discontinuities observed by both ACE, located at L1, and C3, close to the Earth's bow shock, between 2001 and 2012.

[37] We found that by using the fixed set of parameters $\tau_1{}^m = 2$ min, $\tau_2{}^m = 4$ min, $\tau_3{}^m = 5.33$ min, and $\tau_4{}^m = 8.33$ min, the fraction of discontinuities estimated to arrive at C3 within ± 2 min from the observed time delay ($f_{2\text{–min}}$) is 45% for CP, 35.5% for MVAB, and 47.5% for the MVAB0 method. These results are in good agreement with the study by *Mailyan et al.* [2008], which also found that the best method to obtain accurate propagation delays for solar wind discontinuities is MVAB0. By tuning the method parameters for each discontinuity individually, we can determine the optimum set of method parameters. We found that $f_{2\text{–min}}$ increases significantly, up to 69% for CP, 65% for MVAB, and 58% for MVAB0.

[38] Wavelet denoising was used to remove small-scale fluctuations from magnetic measurements, which are known to influence the estimation of the orientation of a discontinuity, thus affecting the time delay estimation. We found that by using a fixed set of denoising parameters for the entire database of discontinuities we obtain only very small

increases of $f_{2-\min}$, if any. By determining the optimum set of denoising parameters for each discontinuity individually, we found that $f_{2-\min}$ increases significantly, up to 74% for CP, 88% for MVAB, and 69% for MVAB0. The fact that MVAB is the most precise method demonstrates that it is more sensitive to small-scale fluctuations than CP or MVAB0, and, by denoising the input signal, we can improve significantly the accuracy of time delay estimation.

[39] When the denoising is applied with a fixed set of parameters, it does not have a significant impact on the statistics of the time delays of solar wind discontinuities in our database. Nevertheless, the denoising has a clear positive effect when applied on variable time intervals as demonstrated by the results obtained for the case study presented in section 5 and by the individually optimized denoising results presented in Figure 8. The case study shows that denoising improves the accuracy of discontinuity determination and allows for an increased eigenvalue ratio threshold, resulting in better overall data quality and the inclusion of a large number of events that originally did not meet the quality criteria, thus improving the statistics.

[40] **Acknowledgments.** The research leading to these results has received funding from the ESA PECS Project KEEV (97049) and from the European Community's Seventh Framework Programme (FP7/2007–2013) under grant agreement 313038 (STORM). C.M. acknowledges the financial support by the Romanian Ministry of Science and Research and by the Wallonie-Bruxelles International through a bilateral collaboration project (593) between the Institute of Space Science (Romania) and the Catholic University of Louvain, and by the Academy of Finland through the HISSI research project 128189. We acknowledge the use of the AMDA science analysis system provided by the Centre de Données de la Physique des Plasmas (CESR, Université Paul Sabatier, Toulouse).

[41] Philippa Browning thanks the reviewers for their assistance in evaluating this paper.

References

Balogh, A., et al. (2001), The Cluster Magnetic Field Investigation: Overview of in-flight performance and initial results, *Ann. Geophys.*, *19*, 1207–1217, doi:10.5194/angeo-19-1207-2001.

Burgess, D., E. Mobius, and M. Scholer (2012), Ion acceleration at the Earth's bow shock, *Space Sci. Rev.*, *173*, 5–47, doi:10.1007/s11214-012-9901-5.

Colburn, D. S., and C. P. Sonett (1966), Discontinuities in the solar wind, *Space Sci. Rev.*, *5*, 439–506, doi:10.1007/BF00240575.

Daubechies, I. (1992), *Ten Lectures on Wavelets*, 377 p., Cbms-Nsf Regional Conference Series in Applied Mathematics, Society for Industrial and Applied Mathematics, Philadelphia, PA, USA.

De Moortel, I., S. Munday, and A. Hood (2004), Wavelet analysis: The effect of varying basic wavelet parameters, *Sol. Phys.*, *222*, 203–228, doi:10.1023/B:SOLA.0000043578.01201.2d.

Donoho, D., and I. M. Johnstone (1995), Adapting to unknown smoothness via wavelet shrinkage, *J. Am. Stat. Assoc.*, *90*, 1200–1224.

Donoho, D. L. (1995), De-noising by soft-thresholding, *IEEE Trans. Inf. Theor.*, *41*(3), 613–627, doi:10.1109/18.382009.

Donoho, D. L., I. M. Johnstone, G. Kerkyacharian, and D. Picard (1995), Wavelet shrinkage: Asymptopia, *J. Roy. Stat. Soc. B*, *57*, 301–369.

Gosling, J. T., J. R. Asbridge, S. J. Bame, G. Paschmann, and N. Sckopke (1978), Observations of two distinct populations of bow shock ions in the upstream solar wind, *Geophys. Res. Lett.*, *5*, 957–960, doi:10.1029/GL005i011p00957.

Haaland, S., and G. Paschmann (2001), Improved boundary normal calculations using minimum variance analysis and wavelet de-noising techniques, in *Proceedings of Les Woolliscroft Memorial Conference,* vol. 492, edited by B. Warmbein, *Eur. Space Agency Spec. Publ.*, pp. 127–132.

Haaland, S., C. Munteanu, and B. Mailyan (2010), Solar wind propagation delay: Comment on "Minimum variance analysis-based propagation of the solar wind observations: Application to real-time global magnetohydrodynamic simulations" by A. Pulkkinen and L. Raststatter, *Space Weather*, *8*, S06005, doi:10.1029/2009SW000542.

Horbury, T. S., D. Burgess, M. Fränz, and C. J. Owen (2001), Three spacecraft observations of solar wind discontinuities, *Geophys. Res. Lett.*, *28*, 677–680, doi:10.1029/2000GL000121.

Jacquey, C., et al. (2010), AMDA, Automated Multi-Dataset Analysis: A web-based service provided by the CDPP, in *The Cluster Active Archive, Studying the Earth's Space Plasma Environment*, edited by H. Laakso et al., 239–247, Springer, Berlin, doi:10.1007/978-90-481-3499-1-16.

Knetter, T. (2005), A new perspective of the solar wind micro-structure due to multi-point observations of discontinuities, Ph.D. thesis, Universitat zu Koln.

Mailyan, B., C. Munteanu, and S. Haaland (2008), What is the best method to calculate the solar wind propagation delay? *Ann. Geophys.*, *26*, 2383–2394, doi:10.5194/angeo-26-2383-2008.

McComas, D. J., S. J. Bame, P. Barker, W. C. Feldman, J. L. Phillips, P. Riley, and J. W. Griffee (1998), Solar Wind Electron Proton Alpha Monitor (SWEPAM) for the advanced composition explorer, *Space Sci. Rev.*, *86*, 563–612, doi:10.1023/A:1005040232597.

Paschmann, G., N. Sckopke, I. Papamastorakis, J. R. Asbridge, S. J. Bame, and J. T. Gosling (1981), Characteristics of reflected and diffuse ions upstream from the Earth's bow shock, *J. Geophys. Res.*, *86*, 4355–4364, doi:10.1029/JA086iA06p04355.

Pulkkinen, A., and L. Rastätter (2009), Minimum variance analysis-based propagation of the solar wind observations: Application to real-time global magnetohydrodynamic simulations, *Space Weather*, *7*, S12001, doi:10.1029/2009SW000468.

Rème, H., et al. (2001), First multispacecraft ion measurements in and near the Earth's magnetosphere with the identical Cluster Ion Spectrometry (CIS) experiment, *Ann. Geophys.*, *19*, 1303–1354, doi:10.5194/angeo-19-1303-2001.

Smith, C. W., J. L'Heureux, N. F. Ness, M. H. Acuña, L. F. Burlaga, and J. Scheifele (1998), The ACE magnetic fields experiment, *Space Sci. Rev.*, *86*, 613–632, doi:10.1023/A:1005092216668.

Sonnerup, B. U. Ö., and M. Scheible (1998), Minimum and maximum variance analysis, in *Analysis Methods for Multi-spacecraft Data*, edited by G. Paschmann and P. W. Daly, chap. 8, pp. 185–220, SR-001 in ISSI Scientific Reports Series, ESA/ISSI, ESA Publ. Div., Noordwijk, Netherlands.

Torrence, C., and G. P. Compo (1998), A practical guide to wavelet analysis, *Bull. Am. Meteorol. Soc.*, *79*, 61–78, doi:10.1175/1520-0477(1998)079<0061:APGTWA>2.0.CO;2.

Weimer, D. R., and J. H. King (2008), Improved calculations of interplanetary magnetic field phase front angles and propagation time delays, *J. Geophys. Res.*, *113*, A01105, doi:10.1029/2007JA012452.